Chinese Journal of Natural Medicines

Structurally diverse rhamnofolane, tigliane, and daphnane diterpenoids from *Euphorbia wallichii* as anti-liver fibrosis agents

Fangyu Yuan, Xinying Zhu, Shuqi Wu, Long Ling, Dong Huang, Lu Gan, Jialuo Huang, Yiling Liao, Guihua Tang, Sheng Yin

Citation: Fangyu Yuan, Xinying Zhu, Shuqi Wu, Long Ling, Dong Huang, Lu Gan, Jialuo Huang, Yiling Liao, Guihua Tang, Sheng Yin, Structurally diverse rhamnofolane, tigliane, and daphnane diterpenoids from *Euphorbia wallichii* as anti-liver fibrosis agents, Chinese Journal of Natural Medicines, 2026, 24(2), 247-256. doi: 10.1016/S1875-5364(26)61095-3.

View online: https://doi.org/10.1016/S1875-5364(26)61095-3

Chinese Journal of Natural Medicines 24 (2026) 247-256

Contents lists available at ScienceDirect

Chinese Journal of Natural Medicines

journal homepage: www.cjnmcpu.com/

Original article

Structurally diverse rhamnofolane, tigliane, and daphnane diterpenoids from *Euphorbia wallichii* as anti-liver fibrosis agents

Fangyu Yuan[Δ], Xinying Zhu[Δ], Shuqi Wu, Long Ling, Dong Huang, Lu Gan, Jialuo Huang, Yiling Liao, Guihua Tang, Sheng Yin[*]

School of Pharmaceutical Sciences, Sun Yat-sen University, Guangzhou 510006, China

ARTICLE INFO

Article history:
Received 3 January 2025
Revised 25 March 2025
Accepted 8 June 2025
Available online 20 February 2026

Keywords:
Euphorbia wallichii
Diterpenoids
Rhamnofolanes
Tiglianes
Daphnanes
Liver fibrosis

ABSTRACT

Twelve new diterpenoids, euphorwallnoids A–L (**1**–**12**), comprising five rhamnofolanes (**1**–**5**), five tiglianes (**6**–**10**), and two daphnanes (**11** and **12**), along with six known analogues (**13**–**18**), were isolated from the whole plants of *Euphorbia wallichii* (*E. wallichii*). Their structures were determined using spectroscopic analysis, computational methods, chemical derivatization, and single-crystal X-ray diffraction. Euphorwallnoid A (**1**) features an unusual 5/7/6/5-tetracyclic scaffold, whereas **2**–**5** represent a rare subclass of 4-deoxygenated rhamnofolanes and **6**–**8** constitute 13-deoxygenated tiglianes. Notably, compound **1** demonstrated promising anti-liver fibrosis activity by significantly inhibiting the expression of fibronectin (FN), *α*-smooth muscle actin (*α*-SMA), and collagen I in transforming growth factor β1 (TGF-β1)-stimulated LX-2 cells at micromolar concentrations.

1. Introduction

Liver fibrosis is a wound-healing response triggered by prolonged organ injuries, often resulting from viral infections, alcohol abuse, autoimmune and metabolic disorders, and cholestasis [1, 2]. Persistent liver fibrosis can lead to distorted hepatic architecture, liver dysfunction, cirrhosis, and ultimately hepatocellular carcinoma or death, imposing a substantial disease burden on both individuals and society [3]. Although numerous potential anti-fibrotic agents have demonstrated significant efficacy in experimental animal models, their effectiveness in clinical trials has been limited or negligible [4, 5]. Therefore, the development of effective anti-liver fibrosis agents remains an urgent unmet need.

Diterpenoid natural products have proven to be a valuable source of "privileged structures" in drug discovery [6, 7]. For example, the naturally occurring tigliane diterpenoid prostratin is a promising preclinical candidate for the treatment of HIV infection [7]. Langduin A, a rhamnofolane-type diterpenoid, has been identified as an active *α*-glucosidase inhibitor with superior activity compared to the clinical drug acarbose [8]. Resiniferatoxin, a member of the daphnane family, exhibits strong desensitization effects on the transduction of painful stimuli, making it highly promising for the treatment of chronic pain [9, 10]. Notably, these three diterpenoids—sharing the same 5/7/6-fused ring system—are all isolated from plants of the *Euphorbia* genus.

In a prior study, we found that 12-deoxyphorbol 13-palmitate [11] and daphnepedunin A [12], both containing the 5/7/6 carbon skeleton, showed potential in an anti-fibrotic screening campaign. *Euphorbia wallichii* (*E. wallichii*) is a perennial shrub distributed in northwest China [13]. Its roots are widely used in traditional Chinese medicine for treating edema, furuncle, exanthema, and cutaneous anthrax [13]. Previous phytochemical investigations revealed that this species is rich in diterpenoids possessing the 5/7/6 carbon ring system [14-16], which prompted our interest. In our ongoing search for anti-liver fibrosis diterpenoids from this plant and to comprehensively characterize the structural diversity of such compounds in *E. wallichii*, we conducted a structure-oriented isolation, leading to the identification of 12 new diterpenoids and 6 known analogues (Fig. 1). Their structures were elucidated through spectroscopic data analysis, quantum chemical calculations, chemical correlations, and single-crystal X-ray diffraction. Herein, we report the isolation, structural characterization, putative biosynthetic pathways, and anti-liver fibrosis activities of these diterpenoids.

2. Results and discussion

2.1. Isolation and structure elucidation

The air-dried powder of the whole plants of *E. wallichii* was extracted with 95% EtOH at room temperature to yield a crude extract, which was then suspended in H_2O and partitioned with EtOAc. The EtOAc-soluble fraction was subjected to solid-phase extraction and eluted sequentially with petroleum ether (PE), CH_2Cl_2, and EtOAc. Various column chromatographic separations

* Corresponding author.
E-mail address: yinsh2@mail.sysu.edu.cn (S. Yin)
Δ These authors contributed equally to this work.

https://doi.org/10.1016/S1875-5364(26)61095-3

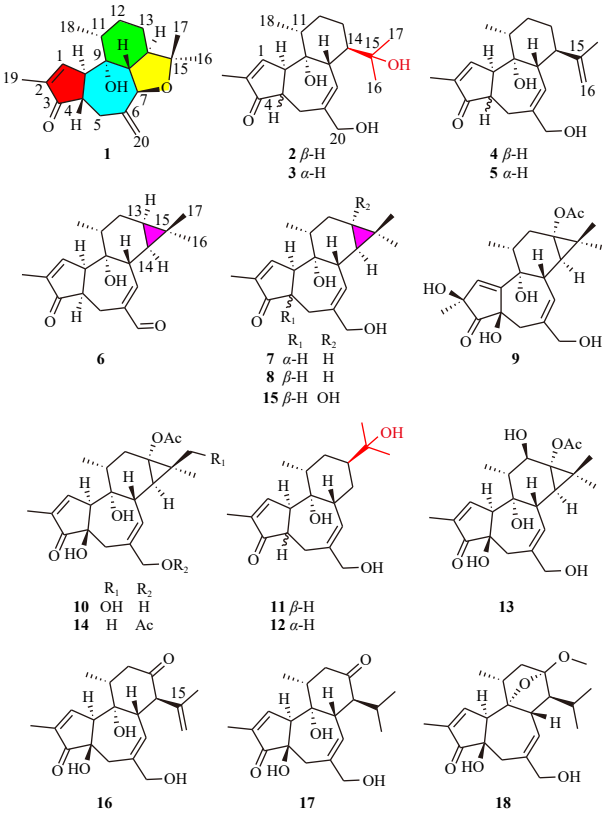

Fig. 1 Chemical structures of compounds **1**–**18**.

of the CH_2Cl_2-eluting fraction yielded compounds **1**–**18**, among which **1**–**12** were new (Fig. 1).

Euphorwallnoid A (**1**) was obtained as colorless crystals. Its molecular formula $C_{20}H_{28}O_3$ was determined by high-resolution electrospray ionization mass spectrometry (HR-ESI-MS), showing an ion at *m/z* 339.1932 $[M + Na]^+$ (Calcd. 339.1931), corresponding to seven degrees of unsaturation. IR absorption bands indicated the presence of hydroxyl (3490 cm^{-1}) and carbonyl (1697 cm^{-1}) functionalities. The ^1H nuclear magnetic resonance (NMR) spectrum displayed signals for four methyl groups [δ_H 0.92 (d, *J* = 6.3 Hz), 1.03 (s), 1.30 (s), and 1.77 (s)], one oxymethine proton [δ_H 4.41 (d, *J* = 9.9 Hz)], three olefinic protons [δ_H 7.51 (s), 4.85 (d, *J* = 1.9 Hz), and 5.23 (d, *J* = 1.9 Hz)], and several aliphatic protons (Table 1). The ^{13}C NMR and DEPT spectra resolved 20 carbon resonances, including a ketocarbonyl (δ_C 208.1), four olefinic carbons (δ_C 108.4, 138.8, 149.1, and 157.7), two oxygenated sp^3 tertiary carbons (δ_C 74.0 and 82.4), four methyls, three sp^3 methylenes, and six sp^3 methines (one oxygenated: δ_C 76.9). With three indices of hydrogen deficiency (IHDs) accounted for by one ketocarbonyl and two double bonds, the remaining four IHDs suggested a tetracyclic framework for **1**.

Three spin systems—H-1/H-10/H-4/H_2-5, H_3-18/H-11/H_2-12, and H_2-13/H-14/H-8/H-7—were established *via* ^1H–^1H correlation spectroscopy (COSY) correlations (Fig. 2). These subunits were further connected through heteronuclear multiple bond correlations (HMBCs) (Fig. 2). The HMBCs from the olefinic methyl singlet (H_3-19) to C-1 (sp^2 methine), C-2 (quaternary sp^2 carbon), and C-3 (ketocarbonyl) linked C-1, C-3, and C-19 to C-2. The HMBC from H-4 to C-3 connected C-3 and C-4, while C-5 was linked to the oxygenated sp^3 methine (C-7) *via* C-6 (a quaternary

Table 1 ^1H (400 MHz) and ^{13}C NMR (100 MHz) data of compounds **1**–**3** in $CDCl_3$ (*J* in Hz).

No.	1		2		3	
	δ_H	δ_C, type	δ_H	δ_C, type	δ_H	δ_C, type
1	7.51, s	157.7, CH	7.44, s	159.2, CH	7.20, s	157.2, CH
2		138.8, C		135.7, C		142.8, C
3		208.1, C		210.3, C		212.1, C
4	2.14, ddd (12.6, 4.0, 2.0)	46.1, CH	2.48, m	44.3, CH	2.72, m	49.2, CH
5	3.00, dd (14.8, 2.3)	37.1, CH_2	2.64, dd (16.5, 11.2)	27.0, CH_2	2.99, dd (15.0, 2.0)	27.4, CH_2
	1.94, m		1.98, dd (16.5, 7.3)		2.41, dd (15.0, 5.2)	
6		149.1, C		139.6, C		136.2, C
7	4.41, d (9.9)	76.9, CH	6.08, d (7.0)	123.5, CH	5.80, s	126.7, CH
8	1.74, dd (11.0, 9.9)	60.5, CH	2.12, t (10.8)	50.2, CH	2.08, dd (9.9, 2.3)	46.4, CH
9		74.0, C		77.2, C		76.5, C
10	2.84, m	59.5, CH	3.07, s	55.1, CH	3.43, m	49.6, CH
11	1.51, m	37.6, CH	1.55, m	35.6, CH	1.75, m	39.4, CH
12	1.61, m	32.3, CH_2	1.57, m	31.6, CH_2	1.54, m	29.7, CH_2
	1.45, m		1.49, m			
13	1.64, m	26.1, CH_2	1.77, br d (12.7)	29.2, CH_2	1.30, m	28.9, CH_2
	1.57, m		0.97, m		1.82, m	
14	2.00, ddd (11.0, 11.0, 3.4)	46.9, CH	1.88, t (10.8)	45.4, CH	1.74, m	49.5, CH
15		82.4, C		74.3, C		74.2, C
16	1.30, s	28.0, CH_3	1.18, s	31.4, CH_3	1.20, s	31.6, CH_3
17	1.03, s	24.2, CH_3	1.04, s	22.9, CH_3	1.16, s	24.5, CH_3
18	0.92, d (6.3)	17.4, CH_3	0.91, d (4.4)	18.6, CH_3	1.05, d (6.7)	15.7, CH_3
19	1.77, s	10.3, CH_3	1.71, s	10.3, CH_3	1.78, s	10.4, CH_3
20	5.23, d (1.9)	108.4, CH_2	3.99, d (15.8)	65.7, CH_2	3.95, br s	68.7, CH_2
	4.85, d (1.9)		3.90, d (15.8)			

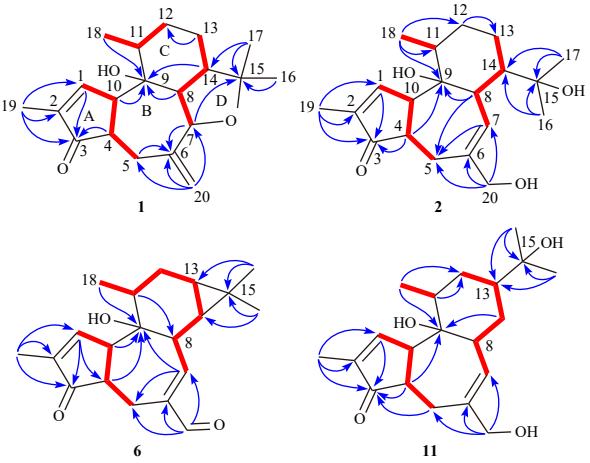

Fig. 2 Key ^{1}H–^{1}H COSY (▬) and HMBC (⟶) correlations of **1**, **2**, **6**, and **11**.

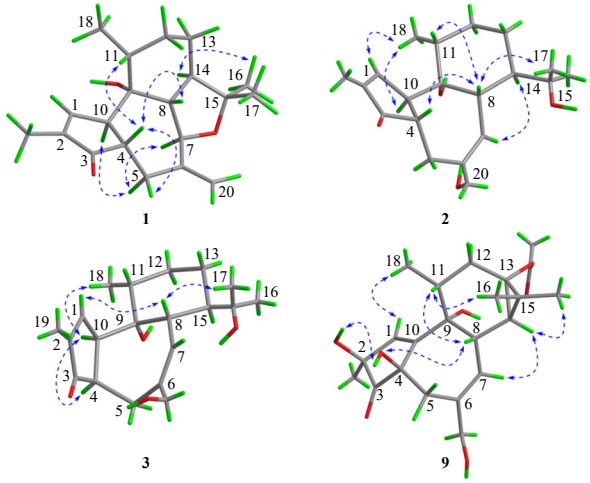

Fig. 3 Key NOE (·····) correlations of **1**–**3** and **9**.

sp^2 carbon), supported by HMBCs from H_2-20 to C-5, C-6, and C-7. HMBCs from H-10 and H-8 to the oxygenated tertiary carbon (C-9) connected C-10 and C-8 to C-9, forming a 5/7 (A/B) fused ring system. C-9 and C-13 were linked to C-11 and C-12, respectively, *via* HMBCs from H_3-18 to C-9 and H_2-13 to C-12, completing a cyclohexane ring (C). An oxygenated isopropyl unit was attached to the sp^3 methine (C-14), as evidenced by HMBCs from H_3-16 and H_3-17 to C-14 and the oxygenated tertiary carbon (C-15). Given the molecule's degree of unsaturation, one additional ring was required. Based on the chemical shifts of the oxygenated tertiary carbon (C-15, δ_C 82.4) and the oxygenated methine (C-7, δ_C 76.9), along with the HMBC from H-7 to C-15, an oxygen bridge between C-7 and C-15 was proposed. Thus, compound **1** was assigned as a rhamnofolane-type diterpenoid featuring an unusual 7,15-oxide bridge.

The relative configuration of **1** was partially determined using nuclear Overhauser effect spectroscopy (NOESY) data (Fig. 3) and ^{1}H–^{1}H coupling constants. Strong NOE interactions between H-4, H-5β, H-8, and H-11 indicated their cofacial arrangement and were arbitrarily assigned as β-oriented. Consequently, the NOE correlations of H-5α/H-10 and H-7 placed these protons in the α-orientation. The large coupling constant between H-8 and H-14 (J = 11.0 Hz) suggested an α-orientation for H-14. The relative configuration at C-14 was further confirmed by gauge-independent atomic orbital (GIAO) calculations of the 1D NMR chemical shifts for the diastereomers 4*S**,7*R**,8*R**,9*S**,10*R**,11*R**,14*R**-**1** (**1a**) and 4*S**,7*R**,8*R**,9*S**,10*R**,11*R**,14*S**-**1** (**1b**) (Fig. 4), performed at the rmpw1pw91/6-31 + g(d, p) level within the polarizable continuum model (PCM) (Supporting Information). DP4 + probability analysis of the experimental and calculated data showed that **1a** (100.00%) was overwhelmingly favored over **1b** (0.00%), confirming 14*R** as the correct relative configuration. Single-crystal X-ray diffraction (Fig. 5) further confirmed the structure and allowed assignment of the absolute configuration as 4*S*,7*R*,8*R*,9*S*,10*R*,11*R*,14*R*.

Euphorwallnoid B (**2**) had a molecular formula of $C_{20}H_{30}O_4$, as determined by HR-ESI-MS (*m/z* 357.2031 [M + Na]$^+$, Calcd. 357.2036). The 1D NMR data of **2** (Table 1) were similar to those of langduin A (**17**) [17]. Detailed 2D NMR analyses revealed key differences: the oxygenated tertiary carbon C-4 (δ_C 74.7) in **17** was replaced by a methine (δ_C 44.3; δ_H 2.48) in **2**, as indicated by ^{1}H–^{1}H COSY correlations of H-1/H-10/H-4/H_2-5 and the HMBC of H-4/C-3 (Fig. 2); the keto carbon C-13 (δ_C 213.1) in **17** was reduced to a methylene (δ_C 29.2) in **2**, supported by ^{1}H–^{1}H COSY correlations of H_2-13/H-14; and the methine (C-15, δ_C 29.0) in **17** was replaced by an oxygenated tertiary carbon (C-15, δ_C 74.3) in **2**, as shown by HMBCs from H_3-16 and H_3-17 to C-15 (Fig. 2).

The relative configuration of **2** was determined by NOESY experiments and analysis of ^{1}H–^{1}H coupling constants. NOE correlations between H-8, H-4, H-11, and H_3-17 indicated that H-4, H-8, H-11, and the C-14–C-15 bond were cofacial and arbitrarily assigned as β-oriented, whereas the NOE correlation of H_3-18/H-10 placed H-10 in the α-orientation (Fig. 3). The large coupling constant $J_{H\text{-}8,14}$ (10.8 Hz) further supported the α-orientation of H-14. The absolute configuration was assigned by electronic circular dichroism (ECD) calculation using time-dependent density functional theory (TDDFT) (Supporting Information). The experimental ECD spectrum of **2** exhibited negative, positive, and negative Cotton effects at 310, 225, and 208 nm (Fig. 6), respectively, matching well with the calculated spectrum for (4*S*,8*R*,9*R*,10*R*,11*R*,14*R*)-**2** (**2a**), indicating this absolute configuration.

Euphorwallnoid C (**3**) was determined to have the same molecular formula **2**, indicating that it is an isomer. The ^{1}H and ^{13}C NMR spectra of **3** were similar to those of **2**, with distinct chemical shift differences observed in the vicinity of C-4 (C-4: δ_C 49.2 in **3** *vs* 44.3 in **2**; C-10: δ_C 49.6 in **3** *vs* 55.1 in **2**; and H_2-5: δ_H 2.99, 2.41 in **3** *vs* 2.64, 1.98 in **2**), suggesting that **3** is a 4-epimer of **2** (Table 1). This structural assignment was further supported by NOE correlations (Fig. 3): the H-4/H-8 correlation in **2** was replaced by H-4/H-10 in **3**, indicating an α-orientation for H-4 in **3**.

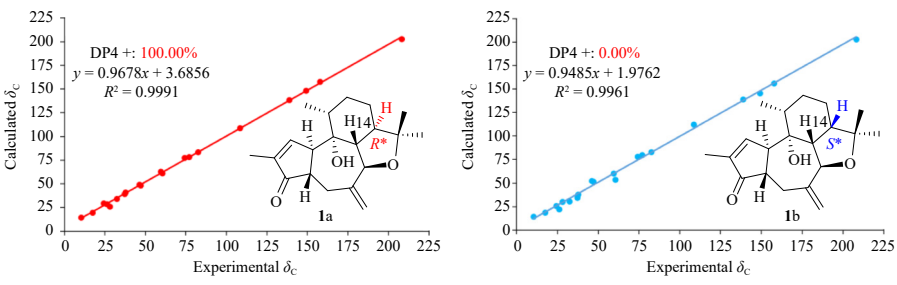

Fig. 4 NMR calculations with DP4 + probability analyses for **1**.

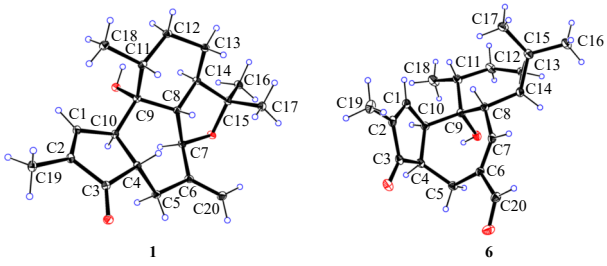

Fig. 5 X-ray draw of compounds **1** and **6** (displacement ellipsoids are drawn at the 20% probability level).

The absolute configuration of (4*R*,8*R*,9*R*,10*R*,11*R*,14*R*)-**3** was assigned using the same ECD protocol (Fig. 6).

Euphorwallnoids D (**4**) and E (**5**) shared the identical molecular formula $C_{20}H_{28}O_3$ based on HR-ESI-MS. Their 1D NMR data (Table 2) closely resembled those of euphorwallside H and I [15], except for the absence of glucose signals, indicating **4** and **5** are the aglycones of euphorwallsides H and I, respectively. The upfield-shifted C-20 signals (δ_C 67.5 in **4**, 70.0 in **5**, 75.8 in euphorwallside H, and 79.3 in euphorwallside I) further supported this conclusion (Fig. S1). The stereochemistry of **4** and **5** was based on comparison with the aglycone moieties of euphorwallside H and II, respectively. This assignment was supported by highly comparable 1D NMR data (Table 2), NOE correlations (Fig. S2), and ECD spectra (Fig. 7).

Euphorwallnoid F (**6**), obtained as colorless crystals, had a molecular formula of $C_{20}H_{26}O_3$, determined by HR-ESI-MS (*m/z* 337.1782 $[M + Na]^+$, Calcd. 337.1774). The 1D NMR data (Table 2) were similar to those of 13-(2,3-dimethylbutyroxy)-4,12-dideoxy-4-*epi*-phorbaldehyde [18], except for the absence of signals for the 2,3-dimethylbutyryl group and an oxygenated tertiary carbon, and the presence of a methine carbon (C-13, δ_C 19.4). This was supported by ^1H–^1H COSY cross-peaks of H_2-12/H-13/H-14 and HMBCs from H_3-16 and H_3-17 to C-13 (Fig. 2). The relative configuration was assigned as identical to the known compound [18] by comparison of 1D NMR and NOESY data (Fig. S2). Specifically, the NOE interaction between H-13 and H-14 (Fig. S2), combined with their large coupling constant (J = 8.9 Hz) [19], indicated a *cis* relationship in the cyclopropane ring. The structure was confirmed by X-ray diffraction (Fig. 5), which also established the absolute configuration as (4*R*,8*S*,9*R*,10*R*,11*R*,13*R*,14*R*).

Euphorwallnoid G (**7**) had a molecular formula of $C_{20}H_{28}O_3$ based on HR-ESI-MS ($[M + Na]^+$ *m/z* 339.1935, Calcd. 339.1931). Compound **7** was spectroscopically similar to **6**, except that the formyl group (δ_H 9.30; δ_C 194.4, C-20) in **6** was replaced by a hydroxymethylene group [δ_H 3.98 (1H, d, J = 12.0 Hz, H-20a) and 3.90 (1H, d, J = 12.0 Hz, H-20b); δ_C 69.5] in **7**, indicating **7** is a formyl-reduced derivative of **6** (Table 3). The structure was confirmed by chemical transformation of **7** to **6** *via* Dess-Martin oxidation (Scheme 1).

Euphorwallnoid H (**8**) had a molecular formula of $C_{20}H_{28}O_3$ from HR-ESI-MS (*m/z* 339.1941 $[M + Na]^+$, Calcd. 339.1931). Its spectroscopic data (Table 3) resembled those of euphorwallside A [15], except for the absence of a glucose moiety, indicating that **8** is the aglycone of euphorwallside A. This was confirmed by the upfield-shifted C-20 signal ($\Delta\delta_C$ 8.2). The stereochemistry was assigned as identical to euphorwallside A based on NOESY correlations (Fig. S2) and ECD spectra (Fig. S3).

Euphorwallnoid I (**9**) had a molecular formula of $C_{22}H_{30}O_7$ from HR-ESI-MS (*m/z* 429.1881 $[M + Na]^+$, Calcd. 429.1884). The NMR signals (Table 3) closely resembled those of prostratin [20], except that the $\Delta^{1(2)}$ double bond migrated to $\Delta^{1(10)}$, and the sp^3 methine was replaced by an oxygenated tertiary carbon (C-2, δ_C 73.8). This was confirmed by HMBCs from H_3-19 (δ_H 1.17) to C-1 (δ_C 136.1), C-2, and C-3, and from H-1 to C-2, C-3, and C-4 (Fig. S1). The relative configuration was assigned from NOESY data (Fig. 3). NOE cross-peaks between 2-OH/4-OH and 4-OH/H-8 suggested these groups were cofacial, with 2-OH assigned as β-oriented. The absolute configuration, 2*S*,4*R*,8*S*,9*R*,11*R*,13*S*,14*R*, was determined by ECD calculation (Fig. S4).

Euphorwallnoid J (**10**) had a molecular formula of $C_{22}H_{30}O_7$ based on HR-ESI-MS (*m/z* 429.1903 $[M + Na]^+$, Calcd. 429.1884). The NMR spectra (Table 4) resembled those of prostratin [20], with the key difference being replacement of the C-17 methyl with an oxymethylene [δ_H 3.57 (d, J = 11.6 Hz) and 3.64 (d, J = 11.6 Hz); δ_C 62.7], indicating **10** is a 17-hydroxylated derivative of prostratin. The stereochemistry was assigned as identical to prostratin based on similar NMR and ECD data (Fig. S3).

Euphorwallnoids K (**11**) and L (**12**) shared the molecular formula $C_{20}H_{30}O_4$ with **2** and **3**, indicating they are isomers. Their NMR data (Table 4) were very similar to **2** and **3**, respectively, differing only in the migration of the C-15–C-16–C-17 (isopropanol) group from C-14 in **2**/**3** to C-13 in **11**/**12**. This was supported by HMBCs from H_3-16 and H_3-17 to C-13 (δ_C 39.1) and ^1H–^1H COSY correlations of H_2-12/H-13/H_2-14/H-8 (Figs. 2 and S1). The relative configurations were assigned as identical to **2** and **3** based on 1D NMR and NOE correlations (Fig. S2). Notably, the NOE correlation of H-8/H_3-17 placed the C-13–C-15 bond in the β-orientation. Absolute configurations were assigned as 4*S*,8*R*,9*R*,10*R*,11*R*,13*R* and 4*R*,8*R*,9*R*,10*R*,11*R*,13*R* using ECD calculations (Figs. S5 and S6).

The known compounds isolated from *E. wallichii* were identified as phorbol 13-monoacetate (**13**) [21], 12-deoxyphorbol-13,20-diacetate (**14**) [22], 4,12-dideoxyphorbol (**15**) [23], crotophorbolone (**16**) [24], langduin A (**17**) [17], and fischerianin A (**18**) [25] by comparison of their NMR data with literature values.

Compound **1** represents only the second natural rhamnofolane diterpenoid reported to contain an unusual 7,15-oxide bridge [26]. The proposed biosynthetic pathway is shown in Scheme 2. Briefly, euphorwallnoid B (**2**), a co-isolated rhamnofolane, serves as the precursor. Protonation at the 20-OH yields intermediate **i**, which dehydrates to form **ii**. Subsequent double bond mi-

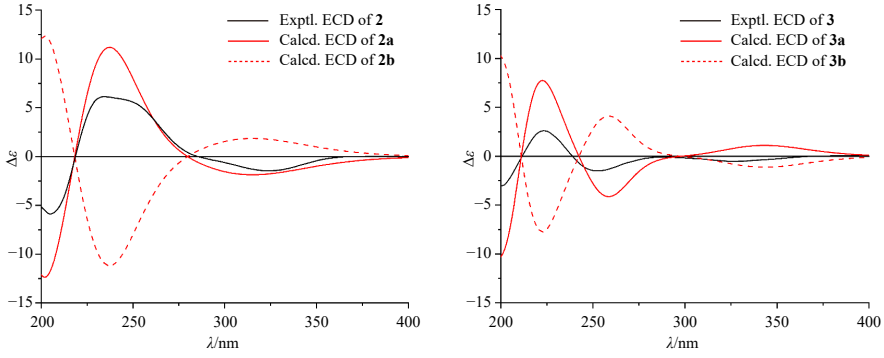

Fig. 6 Experimental and calculated ECD spectra of **2** and **3** in MeCN.

Table 2 ^{1}H and ^{13}C NMR data of compounds **4**–**6** in $CDCl_3$ (*J* in Hz).

No.	**4**[a]		**5**[b]		**6**[a]	
	δ_H	δ_C, type	δ_H	δ_C, type	δ_H	δ_C, type
1	7.48, s	158.7, CH	7.20, s	157.1, CH	7.03, s	155.6, CH
2		136.8, C		142.7, C		143.4, C
3		209.9, C		212.5, C		210.5, C
4	2.61, td (9.8, 4.5)	44.2, CH	2.73, s	49.7, CH	2.82, m	48.8, CH
5	2.81, dd (17.8, 9.4)	29.2, CH_2	3.03, br d (16.3)	25.6, CH_2	3.26, dd (15.4, 4.0)	20.6, CH_2
	2.15, dd (17.8, 9.8)		2.63, dd (16.3, 3.0)		3.00, m	
6		141.5, C		137.4, C		138.9, C
7	5.35, d (5.9)	124.6, CH	5.19, s	125.9, CH	6.18, t (3.3)	154.9, CH
8	2.28, dd (11.8, 6.2)	48.2, CH	1.91, d (12.0)	45.8, CH	2.01, m	42.4, CH
9		77.1, C		77.8, C		75.6, C
10	3.08, m	56.2, CH	3.55, s	49.1, CH	3.53, m	46.7, CH
11	1.61, m	36.3, CH	1.76, m	39.8, CH	1.51, m	36.2, CH
12	1.54, m	31.8, CH_2	1.56, m	29.6, CH_2	1.80, dd (15.3, 6.8)	25.1, CH_2
	1.65, m		1.48, m		1.65, m	
13	1.39, m	31.7, CH_2	1.57, m	32.3, CH_2	0.82, t (8.9)	19.4, CH
	1.63, m		1.36, m			
14	2.43, td (12.1, 2.9)	44.8, CH	2.07, m	48.1, CH	0.41, dd (9.1, 7.7)	24.2, CH
15		147.4, C		147.8, C		18.3, C
16	4.74, br s	112.3, CH_2	4.70, s	112.6, CH_2	1.07, s	28.9, CH_3
	4.76, br s		4.76, s			
17	1.56, s	18.5, CH_3	1.59, s	18.9, CH_3	1.03, s	15.2, CH_3
18	0.95, d (5.9)	18.6, CH_3	1.13, d (5.5)	15.7, CH_3	1.01, d (6.4)	16.2, CH_3
19	1.75, m	10.3, CH_3	1.80, s	10.4, CH_3	1.73, m	10.4, CH_3
20	3.94, d (13.2)	67.5, CH_2	3.96, d (12.4)	70.0, CH_2	9.30, s	194.4, CH
	3.99, d (13.2)		3.87, d (12.4)			

[a] Recorded in 400 MHz for ^{1}H NMR and 100 Hz for ^{13}C NMR; [b] Recorded in 500 MHz for ^{1}H NMR and 125 Hz for ^{13}C NMR.

gration generates resonance hybrid **iii**, followed by nucleophilic addition of the 15-OH to C-7, forming the 7,15-oxide bridged product **1**.

2.2. Screening for potential anti-liver fibrotic compounds on transforming growth factor β1 (TGF-β1)-stimulated fibrosis in LX-2 cells

Given that natural diterpenoids with the 5/7/6 carbon skeleton have significantly contributed to anti-fibrotic agent development [11, 12], compounds **1**–**18**, sharing this core framework, were screened for anti-liver fibrosis activity in TGF-β1-stimulated LX-2 cells. Pirfenidone (PFD, ClinicalTrials.gov identifier: NCT 04099407) served as the positive control. As shown in Fig. 8, TGF-β1 induction significantly increased fibronectin (FN) expression, a hallmark of liver fibrosis [27]. Treatment with compound **1** at 40 μmol·L^{-1} reduced FN levels by over 50%, comparable to PFD at 500 μmol·L^{-1}. No significant cytotoxicity was observed at effective doses (Fig. S7).

*2.3. Compound **1** suppressed the expressions of fibrosis biomarkers FN, α-SMA, and collagen I in TGF-β1-stimulated LX-2 cells*

During liver fibrosis progression, in addition to FN, collagen I (an ECM protein) and α-smooth muscle actin (α-SMA) in hepatic stellate cells (HSCs) are major biomarkers [28, 29]. Since compound **1** significantly inhibited FN production, we further examined its effects on FN, α-SMA, and collagen I protein levels. As expected, compound **1** dose-dependently suppressed the expression of FN, collagen I, and α-SMA at 10, 20, and 40 μmol·L^{-1} in TGF-β1-stimulated LX-2 cells (Fig. 9A). Consistently, **1** also downregulated the mRNA levels of these fibrotic markers in a dose-dependent manner (Fig. 9B). These findings suggest that **1** is a promising anti-fibrotic agent.

3. Conclusion

In our continued investigation of structurally diverse diterpenoids from the *Euphorbia* genus, 12 new diterpenoids and 6 known analogues were isolated from the whole plants of *E. wallichii*. Euphorwallnoid A (**1**) represents the second natural rhamnofolane diterpenoid with a 5/7/6/5-tetracyclic scaffold [26], and its biosynthetic pathway is proposed. Compared to its precursor **2**, the 7,15-oxide bridge enhances anti-fibrotic activity, highlighting it as a promising structural motif for future anti-liver fibrosis agent design. Studies investigating its detailed cellular mechan-

Table 3 ^{1}H (400 MHz) and ^{13}C (100 MHz) NMR data of compounds **7**–**9** (*J* in Hz).

No.	**7**[a]		**8**[a]		**9**[b]	
	δ_H	δ_C, type	δ_H	δ_C, type	δ_H	δ_C, type
1	7.08, s	157.2, CH	7.47, s	158.7, CH	6.04, s	136.1, CH
2		143.1, C		138.4, C		73.8, C
3		213.4, C		209.9, C		219.3, C
4	2.77, m	49.9, CH	2.46, ddd (11.6, 8.8, 4.2)	44.1, CH		76.1, C
5	3.27, dd (15.7, 2.6)	25.0, CH_2	2.81, dd (14.0, 8.8)	30.3, CH_2	2.51, m	40.0, CH_2
	2.50, dd (15.7, 5.4)		2.12, dd (14.0, 11.6)		2.40, m	
6		134.9, C		141.0, C		137.6, C
7	5.21, s	128.8, CH	5.52, d (3.5)	127.6, CH	5.58, d (6.9)	130.5, CH
8	1.70, m	41.0, CH	1.98, t (6.0)	41.0, CH	2.46, m	37.9, CH
9		76.1, C		76.8, C		74.4, C
10	3.49, m	47.3, CH	3.09, m	54.3, CH		149.5, C
11	1.42, m	36.7, CH	1.44, m	34.3, CH	1.56, m	36.1, CH
12	1.71, m	25.4, CH_2	1.45, m	26.2, CH_2	2.25, dd (13.4, 5.7)	30.9, CH_2
	1.61, m				1.49, m	
13	0.71, t (8.6)	19.3, CH	0.77, m	18.5, C		63.4, C
14	0.29, dd (7.6, 5.8)	25.2, CH	0.58, t (7.9)	25.2, CH	0.81, d (4.6)	29.4, CH
15		17.8, C		18.3, C		22.7, C
16	1.00, s	29.0, CH_3	1.07, s	28.4, CH_3	1.09, s	22.9, CH_3
17	0.95, s	15.1, CH_3	0.95, s	14.9, CH_3	1.03, s	15.4, CH_3
18	0.99, d (7.2)	16.3, CH_3	0.93, d (6.8)	19.2, CH_3	0.75, d (6.1)	17.1, CH_3
19	1.76, s	10.4, CH_3	1.74, s	10.3, CH_3	1.17, s	24.3, CH_3
20	3.98, d (12.0)	69.5, CH_2	4.00, m	67.8, CH_2	3.67, d (4.6)	67.2, CH_2
	3.90, d (12.0)		3.90, d (13.0)			
OAc						171.9, C
					2.01, s	20.8, CH_3
2-OH					5.23, s	
4-OH					5.52, s	
9-OH					4.57, s	

[a] Recorded in $CDCl_3$; [b] Recorded in DMSO-d_6.

isms are ongoing.

4. Experimental

4.1. General experimental procedures

X-ray data were obtained on a Rigaku XtaLAB Synergy X-ray diffractometer (Poland). Optical rotations were measured using an automatic polarimeter (Rudolph Autopol I, America). IR spectra were recorded on a Tensor 37 infrared spectrophotometer (Bruker, Germany). NMR spectra were acquired on AM-400/500 spectrometers at 25 °C (Bruker, Switzerland). Melting points were determined using an X-4 melting apparatus without correction (Shanghai Precision & Scientific Instrument Co., Ltd., Shanghai, China). HR-ESI-MS was performed on a LCMS-IT-TOF spectrometer (Shimadzu, China). Semipreparative high-performance liquid chromatography (HPLC) was carried out using a Shimadzu LC-20 AT equipped with an SPD-M20A PDA detector (Japan). A YMC-pack ODS-A column (250 mm × 10 mm, S-5 μm, 12 nm) was used for HPLC purification (YMC, Japan). Column chromatography (CC) employed silica gel (100–200 and 300–400 mesh, Qingdao Haiyang Chemical Co., Ltd., Qingdao, China), D101 macroreticular resin (Donghong Chemical Co., Ltd., China), MCI gel (CHP20P, 75–150 μm, Mitsubishi Chemical Industries Ltd., Ja-

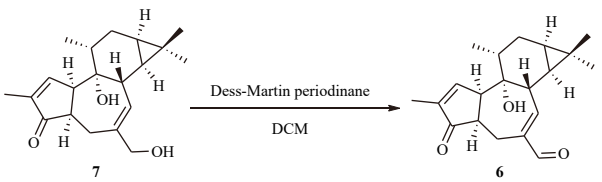

Scheme 1 Chemical transformation of **7** to **6**.

Table 4 ^{1}H (500 MHz) and ^{13}C NMR (125 MHz) data of compounds **10**–**12** (*J* in Hz).

No.	**10**[a]		**11**[b]		**12**[b]	
	δ_H	δ_C, type	δ_H	δ_C, type	δ_H	δ_C, type
1	7.54, s	160.9, CH	7.47, s	156.8, CH	7.13, s	156.8, CH
2		134.9, C		140.7, C		142.0, C
3		210.6, C		209.9, C		211.5, C
4		74.8, C	2.52, m	44.8, CH	2.71, m	49.1, CH
5	2.50, d (19.2)	38.5, CH_2	2.80, dd (18.2, 8.1)	30.2, CH_2	2.84, dd (16.2, 2.5)	26.8, CH_2
	2.42, d (19.2)		2.10, dd (18.2, 11.0)		2.67, dd (16.2, 4.2)	
6		141.9, C		141.0, C		139.1, C
7	5.59, m	130.2, CH	5.31, m	126.9, CH	5.11, s	128.3, CH
8	3.07, t (5.7)	39.9, CH	2.68, m	39.6, CH	2.40, br s	37.7, CH
9		77.4, C		77.1, C		77.2, C
10	3.15, t (2.6)	57.2, CH	2.86, br s	57.4, CH	3.43, br s	50.6, CH
11	2.10, m	37.5, CH	1.79, m	31.8, CH	1.97, m	34.7, CH
12	2.24, dd (13.0, 10.8)	33.1, CH_2	1.50, m	30.1, CH_2	1.50, m	29.9, CH_2
	1.58, dd (10.8, 7.5)		1.20, m			
13		65.1, C	1.91, m	39.1, CH	1.59, m	40.4, CH
14	1.02, d (6.0)	34.2, CH	1.62, m	28.0, CH_2	1.48, m	30.0, CH_2
15		29.7, C		73.0, C		73.5, C
16	1.24, s	18.8, CH_3	1.15, s	26.8, CH_3	1.18, s	28.8, CH_3
17	3.64, d (11.6)	62.7, CH_2	1.15, s	27.1, CH_3	1.16, s	27.2, CH_3
	3.57, d (11.6)					
18	0.91, d (6.5)	19.0, CH_3	1.01, d (7.0)	16.5, CH_3	1.08, d (6.7)	15.3, CH_3
19	1.73, s	10.2, CH_3	1.76, s	10.4, CH_3	1.77, s	10.5, CH_3
20	3.94, d (13.0)	68.2, CH_2	3.98, d (13.0)	67.5, CH_2	3.95, d (13.0)	68.8, CH_2
	3.90, d (13.0)		3.92, d (13.0)		3.99, d (13.0)	
OAc		174.8, C				
	2.06, s	21.1, CH_3				

[a] Recorded in CD_3OD; [b] Recorded in $CDCl_3$.

pan), reversed-phase C_{18} (Rp-C_{18}) silica gel (12 nm, S-50 μm, YMC Co., Ltd., Japan), and Sephadex LH-20 gel (Amersham Biosciences). All solvents were of analytical grade (Guangzhou Chemical Reagents Company, Ltd., Guangzhou, China).

4.2. Plant material

The whole plants of *E. wallichii* Hook. f. were collected from Weixi County, Yunnan Province, China, in July 2020 and authenticated by Prof. Guihua Tang (Sun Yat-sen University). A voucher specimen (accession number: YYFD-202006) has been deposited at the School of Pharmaceutical Sciences, Sun Yat-sen University.

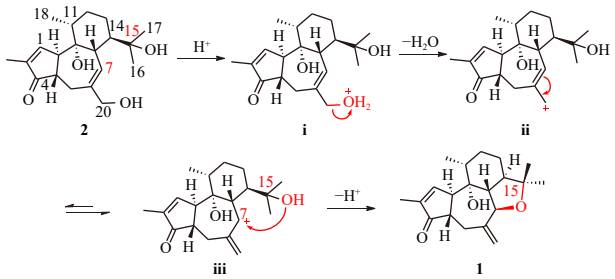

Scheme 2 Proposed biosynthetic pathways for **1**.

4.3. Extraction and isolation

The air-dried powder of whole *E. wallichii* plants (20 kg) was extracted with 95% EtOH (3 × 50 L) at room temperature to afford a crude extract. The crude extract (5.6 kg) was suspended in H_2O and partitioned with EtOAc (3 × 15 L). The EtOAc extract (3000 g) was subjected to solid-phase extraction and eluted with PE, CH_2Cl_2, and EtOAc. The CH_2Cl_2-eluting fraction (450 g) was chromatographed on macroporous resin D101 CC ($MeOH/H_2O$, 30∶70→100∶0) to give six fractions (Frs. I–VI). Fr. III (76 g) was separated by silica gel column (CH_2Cl_2/CH_3OH, 100∶0→1∶1) to afford eight subfractions (Frs. IIIa–IIIh).

Fr. IIIa (15.0 g) was separated by silica gel CC (PE/EtOAc, 100∶0→1∶1) to obtain eight fractions (Frs. IIIa1–IIIa8). Fr. IIIa3 (1.0 g) was subjected to silica gel CC (PE/EtOAc, 100∶1→1∶1),

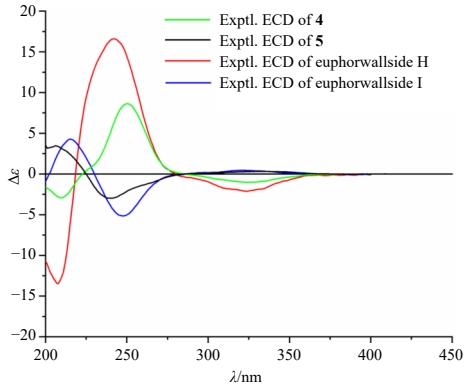

Fig. 7 Experimental ECD spectra of **4**, **5**, euphorwallsides H and I.

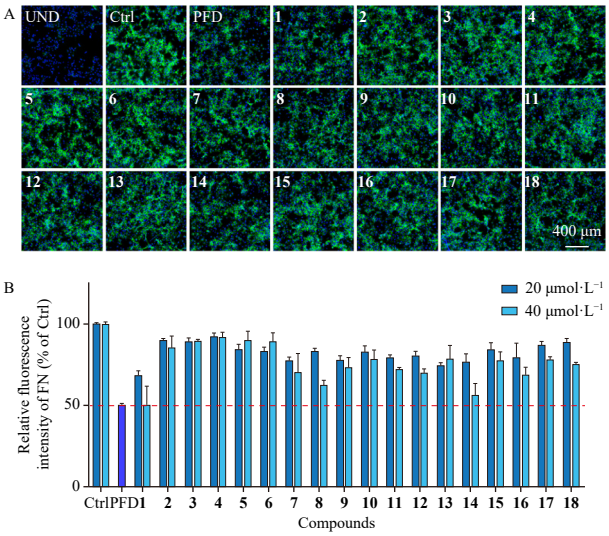

Fig. 8 Inhibitory effects of **1**–**18** on FN levels in TGF-β1-stimulated LX-2 HSCs. (A) Immunofluorescence staining of FN (green) following treatment with **1**–**18** (40 μmol·L^{-1}) and pirfenidone (PFD, 500 μmol·L^{-1}). Cell nuclei were counter-stained with DAPI (blue). (B) Quantitative analysis of FN fluorescence intensity in each treatment group. Data are presented as means ± SEM from three independent experiments. Ctrl, cells treated with TGF-β1; UND, untreated cells; scale bar: 400 μm.

yielding four fractions (Frs. IIIa3a–IIIa3d). Further purification of Fr. IIIa3a (300.0 mg) by HPLC (MeCN/H_2O, 60∶40, 3 mL·min^{-1}) afforded **1** (45.0 mg, t_R 14.3 min). Fr. IIIa5 (2.0 g) was purified by Sephadex LH-20 (MeOH) to give three fractions (Frs. IIIa5a–IIIa5c). Fr. IIIa5a (1.3 g) was chromatographed on silica gel (PE/EtOAc, 20∶1→1∶1), yielding six fractions (Frs. IIIa5a1–IIIa5a6). Fr. IIIa5a6 (120.0 mg) was purified by HPLC (MeCN/H_2O, 70∶30, 3 mL·min^{-1}) to yield **14** (22.0 mg, t_R 9.5 min) and **6** (15.0 mg, t_R 14.3 min).

Fr. IIIc (12.5 g) was subjected to silica gel CC using a gradient of CH_2Cl_2/CH_3OH (100∶0→1∶1) to afford five fractions (Frs. IIIc1–IIIc5). Fr. IIIc3 (1.2 g) was further separated by Rp-C_{18} silica gel CC with a MeOH/H_2O gradient (30∶70→100∶0), yielding nine subfractions (Frs. IIIc3a–IIIc3i). Fr. IIIc3a (80 mg) was loaded onto a Sephadex LH-20 column eluted with MeOH and subsequently purified by HPLC (MeCN/H_2O, 30∶70, 3 mL·min^{-1}) to give compound **10** (15.0 mg, t_R 16.2 min). Fr. IIIc4 (3.0 g) was subjected to Rp-C_{18} silica gel CC (MeOH/H_2O, 30∶70→100∶0), resulting in two fractions (Fr. IIIc4a and Fr. IIIc4b). Fr. IIIc4a (0.75 g) was purified by Sephadex LH-20 (MeOH) to yield **7** (420.0 mg). Fr. IIIc4b (150.0 mg) was purified by HPLC (MeCN/H_2O, 70∶30, 3 mL·min^{-1}) to afford **4** (15.0 mg, t_R 8.5 min) and **5** (10.0 mg, t_R 9.0 min). Fr. IIIc6 (150.0 mg) was separated by silica gel CC (CH_2Cl_2/CH_3OH, 30∶0→10∶1) to obtain **8** (35.0 mg).

Fr. IIIe (6.0 g) was fractionated by silica gel CC using PE/EtOAc (20∶0→1∶3) to yield seven fractions (Frs. IIIe1–IIIe7). Fr. IIIe5 (830 mg) was further separated on a Sephadex LH-20 column (MeOH), affording five subfractions (Frs. IIIe5a–IIIe5e). Fr. IIIe5a (250 mg) was purified by HPLC (MeCN/H_2O, 45∶55, 3 mL·min^{-1}) to yield **12** (30.0 mg, t_R 7.5 min), **9** (10.0 mg, t_R 8.7 min), **15** (23.0 mg, t_R 10.2 min), **16** (26.0 mg, t_R 11.0 min), and **17** (50.0 mg, t_R 13.0 min). Fr. IIIe4 (290 mg) was purified by HPLC (MeCN/H_2O, 25∶75, 3 mL·min^{-1}) to obtain **13** (5.0 mg, t_R 11.0 min), **2** (50.0 mg, t_R 11.8 min), **11** (37.0 mg, t_R 14.8 min), and **3** (45.0 mg, t_R 18.2 min).

4.4. Spectroscopic data

Euphorwallnoid A (**1**): colorless crystals (MeCN), m.p. 196.5–197.5 °C; $[\alpha]_D^{20}$ −23.3 (*c* 0.1, MeCN); ECD (*c* 5.9 × 10^{-4} mol·L^{-1}, MeCN) λ_{max} (Δε) 236 (+17.6), 321 (−2.88); IR (neat) ν_{max} 3490, 2938, 1697, 1017 cm^{-1}; ^{1}H and ^{13}C NMR data (Table 1); HR-ESI-MS *m/z* 339.1932 [M + Na]$^+$ (Calcd. for $C_{20}H_{28}O_3Na$, 339.1931).

Euphorwallnoid B (**2**): yellow oil; $[\alpha]_D^{20}$ +22.3 (*c* 0.1, MeCN); ECD (*c* 6.0 × 10^{-4} mol·L^{-1}, MeCN) λ_{max} (Δε) 205 (−5.89), 235 (+6.15), 324 (−1.46); IR (neat) ν_{max} 3387, 2925, 1690, 1458, 1378, 1021, 735 cm^{-1}; ^{1}H and ^{13}C NMR data (Table 1); HR-ESI-MS *m/z* 357.2031 [M + Na]$^+$ (Calcd. for $C_{20}H_{30}O_4Na$, 357.2036).

Euphorwallnoid C (**3**): brown oil; $[\alpha]_D^{20}$ −44.3 (*c* 0.1, MeCN); ECD (*c* 6.0 × 10^{-4} mol·L^{-1}, MeCN) λ_{max} (Δε) 223 (+2.61), 252 (−1.48), 325 (−0.52); IR (neat) ν_{max} 3386, 2925, 1688, 1376, 1224, 1036, 736 cm^{-1}; ^{1}H and ^{13}C NMR data (Table 1); HR-ESI-MS *m/z* 357.2040 [M + Na]$^+$ (Calcd. for $C_{20}H_{30}O_4Na$, 357.2036).

Euphorwallnoid D (**4**): yellow oil; $[\alpha]_D^{20}$ +28.3 (*c* 0.1, MeCN); ECD (*c* 6.3 × 10^{-4} mol·L^{-1}, MeCN) λ_{max} (Δε) 210 (−2.94), 250 (+8.63), 323 (−1.01); IR (neat) ν_{max} 3418, 2925, 2856, 1694, 1645, 1034, 735 cm^{-1}; ^{1}H and ^{13}C NMR data (Table 2); HR-ESI-MS *m/z* 339.1951 [M + Na]$^+$ (Calcd. for $C_{20}H_{28}O_3Na$, 339.1931).

Euphorwallnoid E (**5**): yellow oil; $[\alpha]_D^{20}$ −3.3 (*c* 0.1, MeCN); ECD (*c* 6.3 × 10^{-4} mol·L^{-1}, MeCN) λ_{max} (Δε) 206 (+3.46), 324 (−2.98), 334 (+0.32); IR (neat) ν_{max} 3420, 2925, 2856, 1689, 1441, 1377, 1261, 1114, 1013, 992, 886 cm^{-1}; ^{1}H and ^{13}C NMR data (Table 2); HR-ESI-MS *m/z* 339.1928 [M + Na]$^+$ (Calcd. for $C_{20}H_{28}O_3Na$, 339.1931).

Euphorwallnoid F (**6**): colorless crystals (MeCN), m.p. 175.3–175.8 °C; $[\alpha]_D^{20}$ −32.0 (*c* 0.1, MeCN); ECD (*c* 3.2 × 10^{-4} mol·L^{-1}, MeCN) λ_{max} (Δε) 227 (−23.78), 320 (+1.89); IR (neat) ν_{max} 3476, 2923, 2863, 1676, 1644, 1634, 1005, 737 cm^{-1}; ^{1}H and ^{13}C NMR data (Table 2); HR-ESI-MS *m/z* 337.1782 [M + Na]$^+$ (Calcd. for $C_{20}H_{26}O_3Na$, 337.1774).

Euphorwallnoid G (**7**): yellow oil; $[\alpha]_D^{20}$ −62.5 (*c* 0.1, MeCN); ECD (*c* 6.3 × 10^{-4} mol·L^{-1}, MeCN) λ_{max} (Δε) 214 (+3.31), 245 (−3.99), 321 (+0.23); IR (neat) ν_{max} 3409, 2924, 1693, 1637, 1374, 1000, 885 cm^{-1}; ^{1}H and ^{13}C NMR data (Table 3); HR-ESI-MS *m/z* 339.1935 [M + Na]$^+$ (Calcd. for $C_{20}H_{28}O_3Na$, 339.1931).

Euphorwallnoid H (**8**): yellow oil; $[\alpha]_D^{20}$ +41.7 (*c* 0.1, MeCN); ECD (*c* 6.3 × 10^{-4} mol·L^{-1}, MeCN) λ_{max} (Δε) 201 (−6.30), 237 (+3.31), 324 (−0.60); IR (neat) ν_{max} 3417, 2923, 1693, 1630, 1376, 1265, 1063, 996, 734 cm^{-1}; ^{1}H and ^{13}C NMR data (Table 3); HR-ESI-MS *m/z* 339.1941 [M + Na]$^+$ (Calcd. for $C_{20}H_{28}O_3Na$, 339.1931).

Euphorwallnoid I (**9**): yellow oil; $[\alpha]_D^{20}$ +32.0 (*c* 0.1, MeCN); ECD (*c* 4.9 × 10^{-4} mol·L^{-1}, MeCN) λ_{max} (Δε) 213 (−1.63), 322 (+0.99); IR (neat) ν_{max} 3373, 2930, 1717, 1263, 734 cm^{-1}; ^{1}H and ^{13}C NMR data (Table 3); HR-ESI-MS *m/z* 429.1881 [M + Na]$^+$ (Calcd. for $C_{22}H_{30}O_7Na$, 429.1884).

Euphorwallnoid J (**10**): yellow oil; $[\alpha]_D^{20}$ +48.7 (*c* 0.1, MeCN); ECD (*c* 4.9 × 10^{-4} mol·L^{-1}, MeCN) λ_{max} (Δε) 205 (−16.26), 229 (+15.27), 269 (−1.48); IR (neat) ν_{max} 3373, 2926, 1702, 1251,

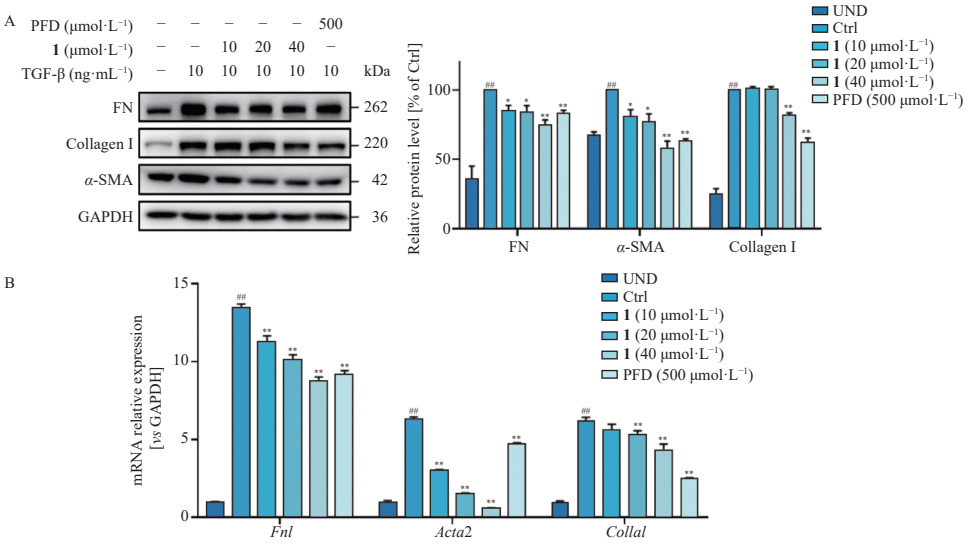

Fig. 9 Compound **1** suppressed the expressions of fibrotic biomarkers FN, α-SMA , and collagen I in TGF-β1-stimulated LX-2 cells. (A) Western blot analysis showing that **1** suppressed the protein levels of FN, collagen I, and α-SMA. (B) qRT-PCR analysis indicating that **1** suppressed the transcript levels of FN (*Fn1*), collagen I (*Col1a1*), and α-SMA (*Acta2*). The mRNA level was normalized to GAPDH and expressed as fold changes relative to the UND. Data are presented as means ± SEM from three independent experiments. Statistical significance was determined by a two-tailed unpaired Student's *t*-test. $^{\#}P < 0.05$, $^{\#\#}P < 0.01$ *vs* untreated (UND) group; $^{*}P < 0.05$, $^{**}P < 0.01$ *vs* TGF-β1 treated (Ctrl) group.

1013, 735 cm^{-1}; ^{1}H and ^{13}C NMR data (Table 4); HR-ESI-MS *m/z* 429.1903 $[M + Na]^+$ (Calcd. for $C_{22}H_{30}O_7Na$, 429.1884).

Euphorwallnoid K (**11**): brown oil; $[\alpha]_D^{20}$ +51.3 (*c* 0.1, MeCN); ECD (*c* 6.0 × 10^{-4} mol·L^{-1}, MeCN) λ_{max} (Δε) 205 (−12.35), 235 (+12.40), 324 (−1.51); IR (neat) ν_{max} 3388, 2969, 2934, 1689, 1379, 998, 734 cm^{-1}; ^{1}H and ^{13}C NMR data (Table 4); HR-ESI-MS *m/z* 357.2043 $[M + Na]^+$ (Calcd. for $C_{20}H_{30}O_4Na$, 357.2036).

Euphorwallnoid L (**12**): brown oil; $[\alpha]_D^{20}$ −34.7 (*c* 0.1, MeCN); ECD (*c* 6.0 × 10^{-4} mol·L^{-1}, MeCN) λ_{max} (Δε) 209 (+4.61), 245 (−3.19), 321 (+0.63); IR (neat) ν_{max} 3397, 2924, 1691, 1377, 1024, 998 cm^{-1}; ^{1}H and ^{13}C NMR data (Table 4); HR-ESI-MS *m/z* 357.2041 $[M + Na]^+$ (Calcd. for $C_{20}H_{30}O_4Na$, 357.2036).

4.5. X-ray crystal structure analysis

Crystallographic data for euphorwallnoid A (**1**): $C_{20}H_{28}O_3$; *M* = 316.42; monoclinic, space group $P2_1$ (No. 4), *a* = 10.059 20 (10) Å, *b* = 17.733 70 (10) Å, *c* = 10.851 10 (10) Å, *β* = 116.9310 (10)°, *V* = 1725.77 (3) $Å^3$, *Z* = 4, *T* = 99.99 (10) K, *μ*(Cu K*α*) = 0.632 mm^{-1}, D_{calc} = 1.218 g·cm^{-3}, 35 753 reflections measured (9.142° ≤ 2Θ ≤ 158.172°), 6931 unique (R_{int} = 0.0694, R_{sigma} = 0.0393) which were used in all calculations. The final R_1 was 0.0415 [I > 2σ (I)] and wR_2 was 0.1112 (all data). Flack parameter = −0.02 (8). Crystallographic data for the structure of **1** have been deposited in the Cambridge Crystallographic Data Centre (CCDC) (deposition number: CCDC 2396517).

Crystallographic data for euphorwallnoid F (**6**): $C_{20}H_{26}O_3$; *M* = 314.41; orthorhombic, space group $P2_12_12_1$ (No. 19), *a* = 8.485 80 (10) Å, *b* = 10.3602 (2) Å, *c* = 19.7314 (3) Å, *V* = 1734.68 (5) $Å^3$, *Z* = 4, *T* = 100.00 (10) K, *μ*(Cu K*α*) = 0.629 mm^{-1}, D_{calc} = 1.204 g·cm^{-3}, 17 692 reflections measured (8.964° ≤ 2Θ ≤ 153.774°), 3591 unique (R_{int} = 0.0853, R_{sigma} = 0.0479) which were used in all calculations. The final R_1 was 0.0491 [I > 2σ (I)] and wR_2 was 0.1289 (all data). Flack parameter = 0.01 (16). Crystallographic data for the structure of **6** have been deposited in the CCDC (deposition number: CCDC 2395529).

4.6. ECD and NMR calculations

The details of NMR calculations for **1** and ECD calculations for **2**, **3**, **9**, **11**, and **12** are provided in the Supporting information.

4.7. Chemical transformation of **7** to **6**

Compound **7** (5.0 mg, 0.016 mmol) was dissolved in CH_2Cl_2 (1 mL) and stirred at room temperature. To this solution, Dess-Martin periodinane (2.0 mg, 0.005 mmol) was added in a single portion. The reaction mixture was stirred at room temperature for 2 h and then evaporated. The crude residue was subjected to silica gel CC (PE/EtOAc, 10∶1) to afford **6** (4.0 mg, 0.013 mmol, 80.57%), which was identified by ^{1}H NMR analysis.

4.8. Biological experiment procedure

The cell culture assay, high-content screening (HCS) assay, real-time quantitative polymerase chain reaction (RT-qPCR) assay, cytotoxicity assay, and Western blot analysis were performed as previously described [30].

Funding

This work was supported by the National Natural Science Foundation of China (Nos. 82404454, 22407144, and 82304322), the China Postdoctoral Science Foundation (No. 2024M753800), the Postdoctoral Fellowship Program of CPSF (No. GZC 20242113), and the Open Program of Shenzhen Bay Laboratory (No. SZBL2021080601007).

Supporting information

Supporting information is available free of charge at: ^{1}H–^{1}H COSY and HMBC correlations of **3**–**5**, **7**–**10**, and **12**; Key NOESY correlations of **4**–**8** and **10**–**12**; NMR calculations for **1**; ECD calculations for **2**, **3**, **9**, **11**, and **12**; NMR, HR-ESI-MS, and IR spectra of **1**–**12**; 1D NMR spectra of **13**–**18**.

Declaration of competing interest

The authors declare no competing financial interest.

References

1 Higashi T, Friedman SL, Hoshida Y. Hepatic stellate cells as key target in liver fibrosis. *Adv Drug Delivery Rev*. 2017;121:27-42. https://doi.org/10.1016/j.addr.2017.05.007.

2 Trautwein C, Friedman SL, Schuppan D, et al. Hepatic fibrosis: concept to treatment. *J Hepatol*. 2015;62:15-24. https://doi.org/10.1016/j.jhep.2014.10.023.

3 Sumeet KA, Harshad D, John E, et al. Burden of liver diseases in the world. *J Hepatol*. 2019;70(1):151-171. https://doi.org/10.1016/j.jhep.2018.09.014.

4 Zhao MY, Wang LQ, Wang MZ, et al. Targeting fibrosis, mechanisms and cilinical trials. *Signal Transduct Target Ther*. 2022;7:206. https://doi.org/10.1038/s41392-022-01070-3.

5 Henderson NC, Rieder F, Wynn TA. Fibrosis: from mechanisms to medicines. *Nature*. 2020;587:555-566. https://doi.org/10.1038/s41586-020-2938-9.

6 Cech NB, Oberlies NH. From plant to cancer drug: lessons learned from the discovery of taxol. *Nat Prod Rep*. 2023;40(7):1153-1157. https://doi.org/10.1039/D3NP00017F.

7 Sánchez-Duffhues G, Vo MQ, Pérez M, et al. Activation of latent HIV-1 expression by protein kinase C agonists. A novel therapeutic approach to eradicate HIV-1 reservoirs. *Curr Drug Targets*. 2011;12:348-356. https://doi.org/10.2174/138945011794815266.

8 Wei YL, Yu ZL, Huo XK, et al. Diterpenoids from the roots of *Euphorbia fischeriana* and their inhibitory effects on α-glucosidase. *J Asian Nat Prod Res*. 2018;20:977-984. https://doi.org/10.1080/10286020.2017.1367923.

9 Brown DC. Resiniferatoxin: the evolution of the "molecular scalpel" for chronic pain relief. *Pharmaceuticals*. 2016;9:47. https://doi.org/10.3390/ph9030047.

10 Szallasi A, Blumberg PM. Resiniferatoxin, a phorbol-related diterpene, acts as an ultra potent analog of capsaicin, the irritant constituent in red pepper. *Neuroscience*. 1989;30:515-520. https://doi.org/10.1016/0306-4522(89)90269-8.

11 Gan L, Jiang QW, Huang D, et al. A natural small molecule alleviates liver fibrosis by targeting apolipoprotein L2. *Nat Chem Biol*. 2025;21(1):80-90. https://doi.org/10.1038/s41589-024-01704-3.

12 Hu XR, Gan L, Tang ZW, et al. A natural small molecule mitigates kidney fibrosis by targeting Cdc42-mediated GSK-3β/β-catenin signaling. *Adv Sci*. 2024;11:2307850. https://doi.org/10.1002/advs.202307850.

13 Flora of China Editorial Committee. *Flora of China*. Vol. 44. Beijing: Science Press; 1997:88.

14 Yang DS, Peng WB, Yang YP, et al. Chemical constituents from *Euphorbia wallichii* and their biological activities. *J Asian Nat Prod Res*. 2015;17:946-951. https://doi.org/10.1080/10286020.2015.1038525.

15 Yuan FY, Tang ZY, Huang D, et al. Tigliane and rhamnofolane glycosides from *Euphorbia wallichii* prevent oxidative stress-induced neuronal death in PC-12 cells. *Bioorg Chem*. 2022;128:106103. https://doi.org/10.1016/j.bioorg.2022.106103.

16 Zhan ZJ, Li S, Chu W, et al. *Euphorbia* diterpenoids: isolation, structure, bioactivity, biosynthesis, and synthesis (2013–2021). *Nat Prod Rep*. 2022;39(11):2132-2174. https://doi.org/10.1039/d2np00047d.

17 Ma QG, Liu WZ, Wu XY, et al. Diterpenoids from *Euphorbia fischeriana*. *Phytochemistry*. 1997;44(4):663-666. https://doi.org/10.1016/S0031-9422(96)00605-X.

18 Shokoohinia Y, Sajjadi SE, Zolfaghari B, et al. Diterpenoid (poly)esters and a ring A-*seco*-phorboid from the aerial parts of *Euphorbia macroclada* Boiss. *Fitoterapia*. 2010;81:884-890. https://doi.org/10.1016/j.fitote.2010.05.015.

19 Tormena CF, Rittner R, Contreras RH, et al. Anomeric effect on germinal and vicinal $J_{H\text{-}H}$ NMR coupling constants. *J Phys Chem A*. 2004;108:7762-7768. https://doi.org/10.1021/jp047226z.

20 Gustafson KR, Cardellina II JH, McMahon JB, et al. A nonpromoting phorbol from the samoan medicinal plant *Homalanthus nutans* inhibits cell killing by HIV-1. *J Med Chem*. 1992;35:1978-1986. https://doi.org/10.1021/jm00089a006.

21 Pieters LAC, Vlietinck AJ. ^{13}C NMR spectroscopy of phorbol esters. *Magn Reson Chem*. 1987;25:368-374. https://doi.org/10.1002/mrc.1260250420.

22 Miana GA, Bashir M, Evans FJ. Isolation of prostratin from *Euphorbia cornigera*. *Planta Med*. 1985;51(4):353-354. https://doi.org/10.1055/s-2007-969515.

23 Karalai C, Wiriyachitra P, Sorg B, et al. Medicinal plants of Euphorbiaceae occurring and utilized in Thailand. V. Skin irritants of the daphnane and tigliane type in latex of *Excoecaria bicolor* and the uterotonic activity of the leaves of the tree. *Phytother Res*. 1995;9:482-488. https://doi.org/10.1002/ptr.2650090704.

24 Wang XH, Liu L, Li J, et al. Chemical constituents of the seed cake of *Jatropha curcas*. *Chem Nat Comp*. 2018;54:606-609. https://doi.org/10.1007/s10600-018-2424-x.

25 Xie RH, Xia GY, Zhu JX, et al. Daphnane-type diterpenoids from *Euphorbia fischeriana* Steud and their cytotoxic activities. *Fitoterapia*. 2021;149:104810. https://doi.org/10.1016/j.fitote.2020.104810.

26 Tchinda AT, Tsopmo A, Tene M, et al. Diterpenoids from *Neoboutonia glabrescens* (Euphorbiaceae). *Phytochemistry*. 2003;64:575-581. https://doi.org/10.1016/S0031-9422(03)00158-4.

27 Lee UE, Friedman SL. Mechanisms of hepatic fibrogenesis. *Best Pract Res Clin Gastroenterol*. 2011;25(2):195-206. https://doi.org/10.1016/j.bpg.2011.02.005.

28 Tsuchida T, Friedman SL. Mechanisms of hepatic stellate cell activation. *Nat Rev Gastroenterol Hepatol*. 2017;14(7):397-411. https://doi.org/10.1038/nrgastro.2017.38.

29 Zollinger AJ, Smith ML. Fibronectin, the extracellular glue. *Matrix Biol*. 2017;61:27-37. https://doi.org/10.1016/j.matbio.2016.07.011.

30 Li S, Gan L, Tian YJ, et al. Presegetane diterpenoids from *Euphorbia sieboldiana* as a new type of anti-liver fibrosis agents that inhibit TGF-β/Smad signaling pathway. *Bioorg Chem*. 2021;114:105222. https://doi.org/10.1016/j.bioorg.2021.105222.